PNAS
www.pnas.org

Supplementary Information for

Loss of TDP-43 in astrocytes leads to motor deficits by triggering A1-like reactive phenotype and exerting non-cell-autonomous toxicity

Audrey Yi Tyan Peng[1,*], Ira Agrawal[1,*], Wan Yun Ho[1,*], Yi-Chun Yen[1,#], Ashley J. Pinter[1], Jerry Liu[1], Qi Xuan Cheryl Phua[1], Katrianne Bethia Koh[1], Jer-Cherng Chang[1], Emma Sanford[1], Jodie Hon Kiu Man[1], David H. Gutmann[2], Peiyan Wong[3,4], Greg Tucker-Kellogg[5,6], Shuo-Chien Ling[1,4,7,8]

Author for correspondence: Shuo-Chien Ling
Email: shuochien@gmail.com or phsling@nus.edu.sg

This PDF file includes:

Figures S1 to S10
Tables S1 to S3
SI References

Other supplementary materials for this manuscript include the following:

Datasets S1 to S2

Supplementary Information

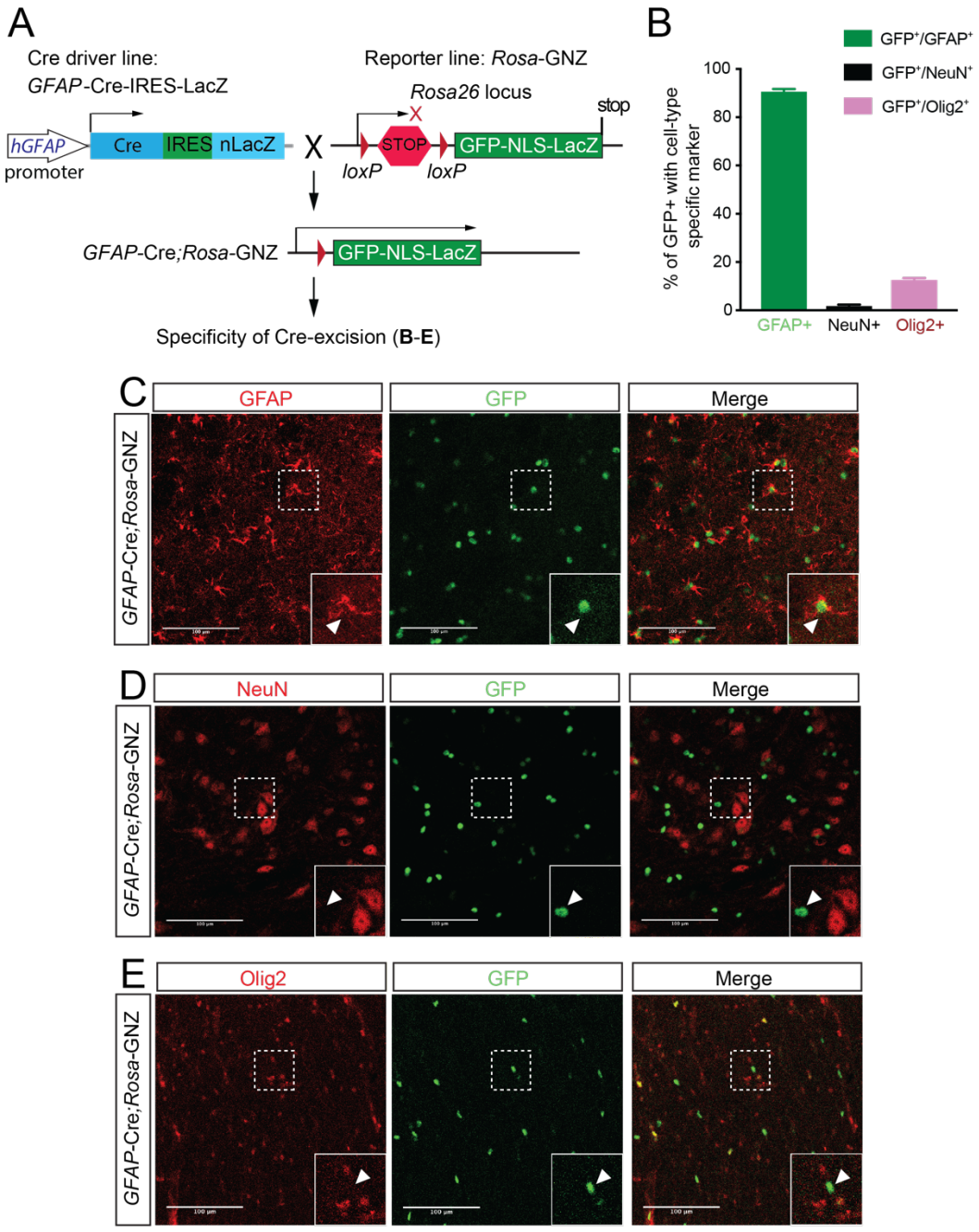

Fig. S1. GFAP-Cre activity is restricted to astrocytes in spinal cord

Fig. S1. Cre-mediated recombination is largely restricted to astrocytes in the spinal cord of *GFAP*-Cre mice. (A) Assessment of *GFAP*-Cre-specificity by crossing the *GFAP*-Cre driver line with a *Rosa26*-GNZ reporter line. Schematics outlining the mating strategy used to obtain *GFAP-Cre*;*Rosa26*-GNZ mice and subsequent analysis. (B) Quantification of GFP with cell-type specific markers: GFAP (astroyctes), NeuN (neurons) and Olig2 (oligodendrocyte lineage cells). (C-E) Confocal images of GFP double labeling with cell type-specific markers. GFP signals co-localized with astrocyte marker GFAP (C), but not with neuronal marker NeuN (D), or oligodendrocyte lineage cell marker Olig2 (E) in *GFAP-Cre*;*Rosa26*-GNZ spinal cord. Scale bar = 100 μm.

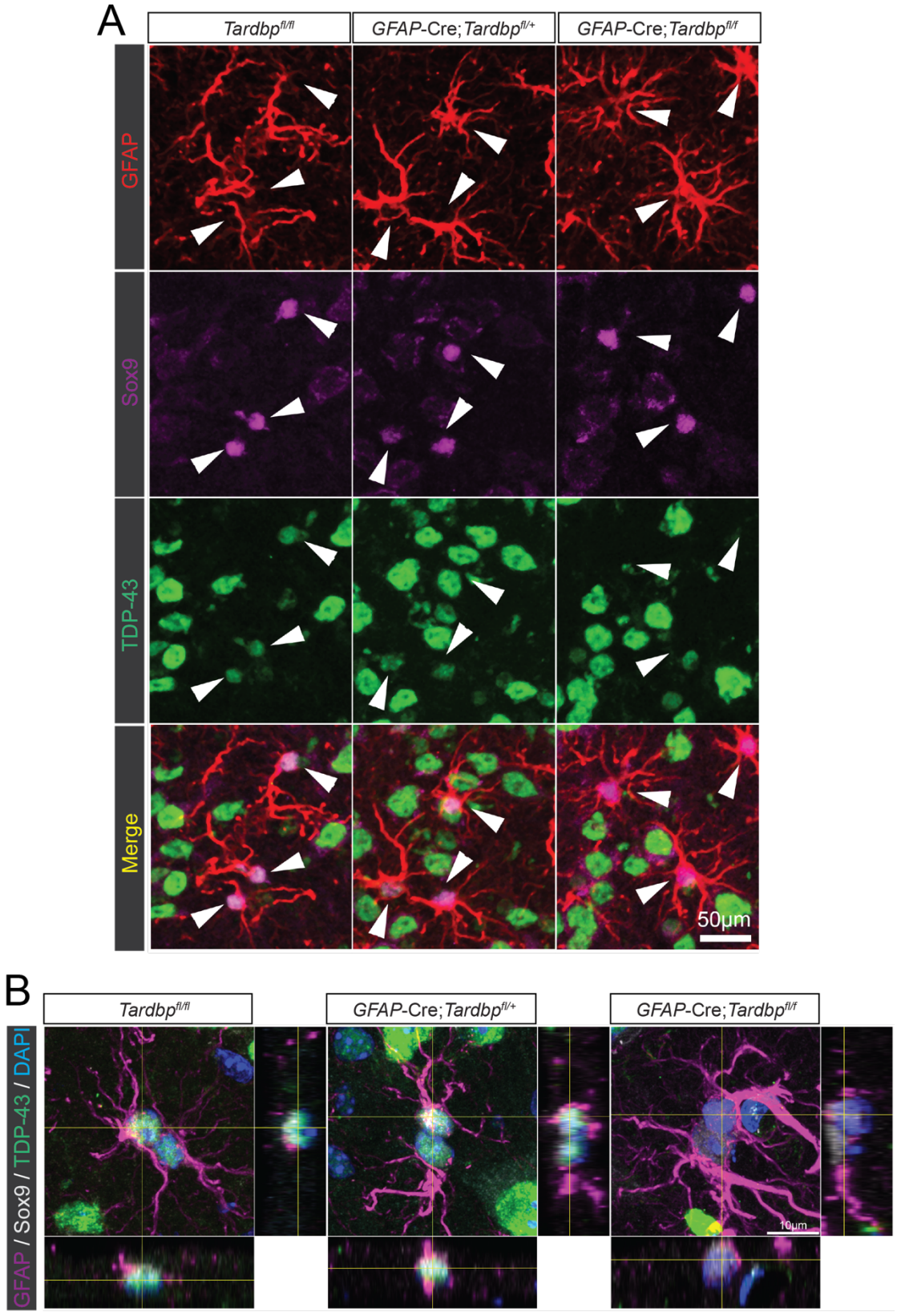

Fig. S2. Selective TDP-43 deletion in astrocytes

Fig. S2. Deletion of TDP-43 in astrocytes. (A) Confocal image of grey matter of lumbar spinal cord of *Tardbp*$^{fl/fl}$ (ctr), *GFAP-Cre*;*Tardbp*$^{fl/+}$ (cHet), *GFAP-Cre*;*Tardbp*$^{fl/fl}$ (cKO) mice immuno-stained with astrocyte markers, GFAP (red) and Sox9 (magenta), and TDP-43 (green). Arrowhead points to GFAP/Sox9-double positive astrocytes. Scale bar= 50 µm. (B) Orthogonal view of 60 day old spinal cord sections co-labelled for astrocytes (GFAP^{+}, red) and TDP-43 (green) markers for the three genotypes. Astrocyte activation is evident in *GFAP-Cre*;*Tardbp*$^{fl/fl}$ mice. Scale bar = 10 µm.

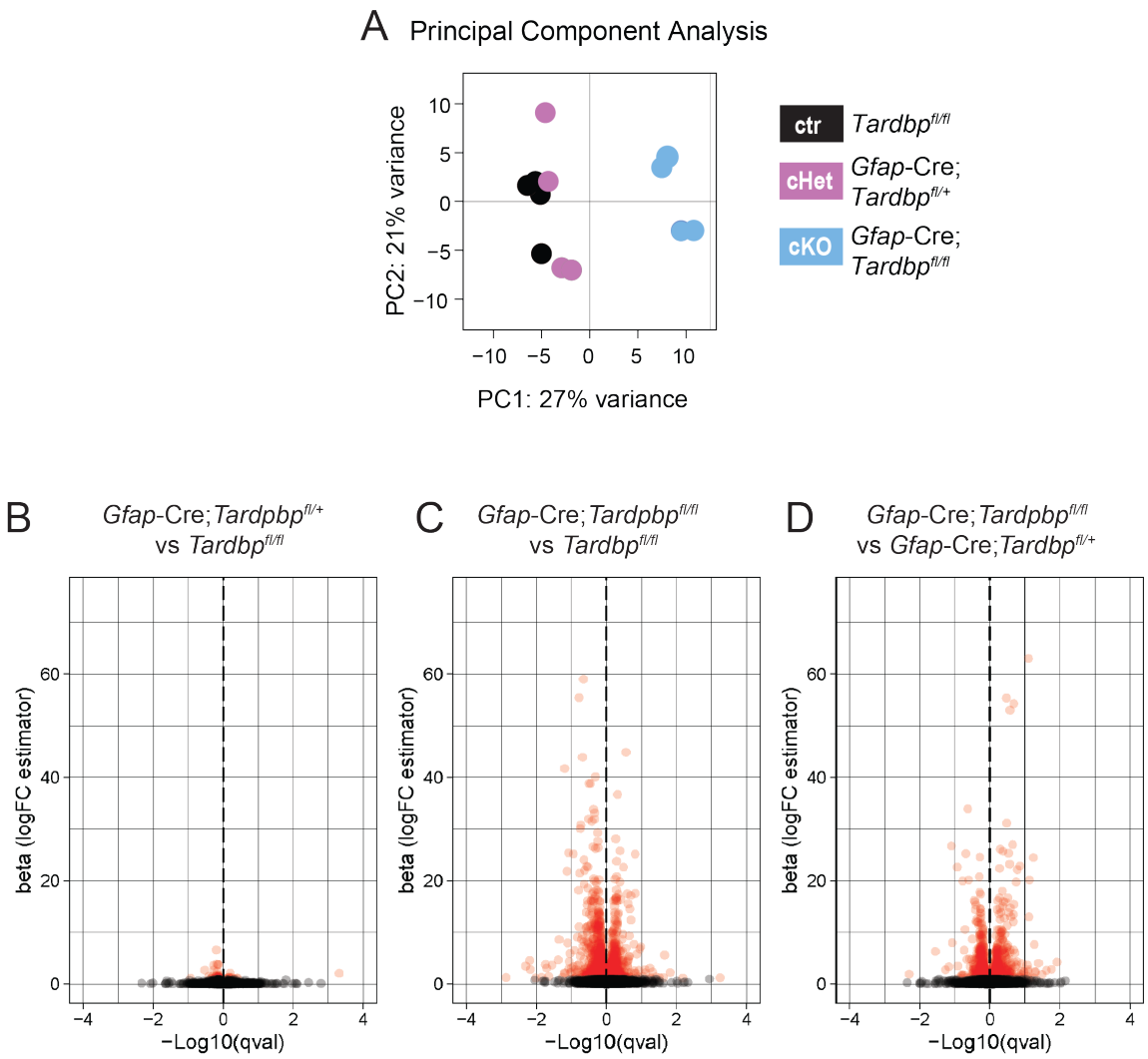

Fig. S3. Distinct transcriptomic changes in the spinal cords of mice with astroglial TDP-43 deletion

Fig. S3. Distinct transcriptomic changes in the spinal cords of mice with astroglial TDP-43 deletion. (A) Principal Component Analysis of *Tardbp*$^{fl/fl}$ (ctr), *GFAP-Cre*;*Tardbp*$^{fl/+}$ (cHet), *GFAP-Cre*;*Tardbp*$^{fl/fl}$ (cKO) mouse spinal cord RNA-Seq samples revealed grouping of cKO samples separate from ctr and cHet samples along the first two principal components. (B-D) Volcano plots depicting the gene expression changes and significance of pairwise comparisons of (B) *GFAP-Cre*;*Tardbp*$^{fl/+}$ (cHet) vs *Tardbp*$^{fl/fl}$ (ctr) samples, (C) *GFAP-Cre*;*Tardbp*$^{fl/fl}$ (cKO) vs *Tardbp*$^{fl/fl}$ (ctr) samples, and (D) *GFAP-Cre*;*Tardbp*$^{fl/fl}$ (cKO) vs *Cre*;*Tardbp*$^{fl/+}$ (cHet) samples. Genes which are significantly differentially expressed at *q*-value < 0.1 are in red.

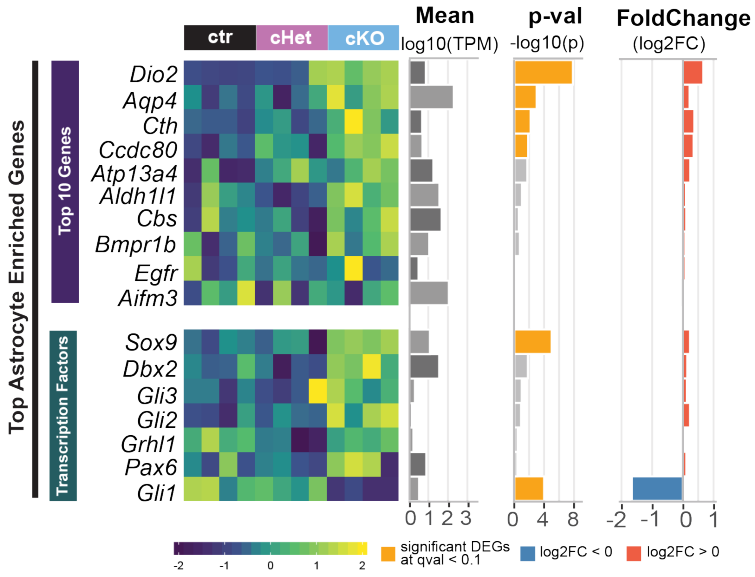

Fig. S4. No apparent up-regulations of astrocyte-enriched genes

Fig. S4. Normal expression levels for astrocyte-enriched genes in mice with astroglial TDP-43 deletion. Heat map of the expression level of top cell-type enriched genes and transcription

factors for astrocytes in *Tardbp*$^{fl/fl}$ (ctr), *GFAP-Cre*;*Tardbp*$^{fl/+}$ (cHet) and *Cre*;*Tardbp*$^{fl/fl}$ (cKO) samples, along with their mean expression level across all samples (log10(TPM)), and *p*-value (-log10(*p*-value)) and fold change (log2(FoldChange)) in *GFAP-Cre*;*Tardbp*$^{fl/fl}$ (cKO) samples as compared to *Tardbp*$^{fl/fl}$ (ctr) samples. Positive and negative fold changes are coloured red and blue respectively and *p*-values corresponding to significant *q*-values < 0.1 are coloured in yellow.

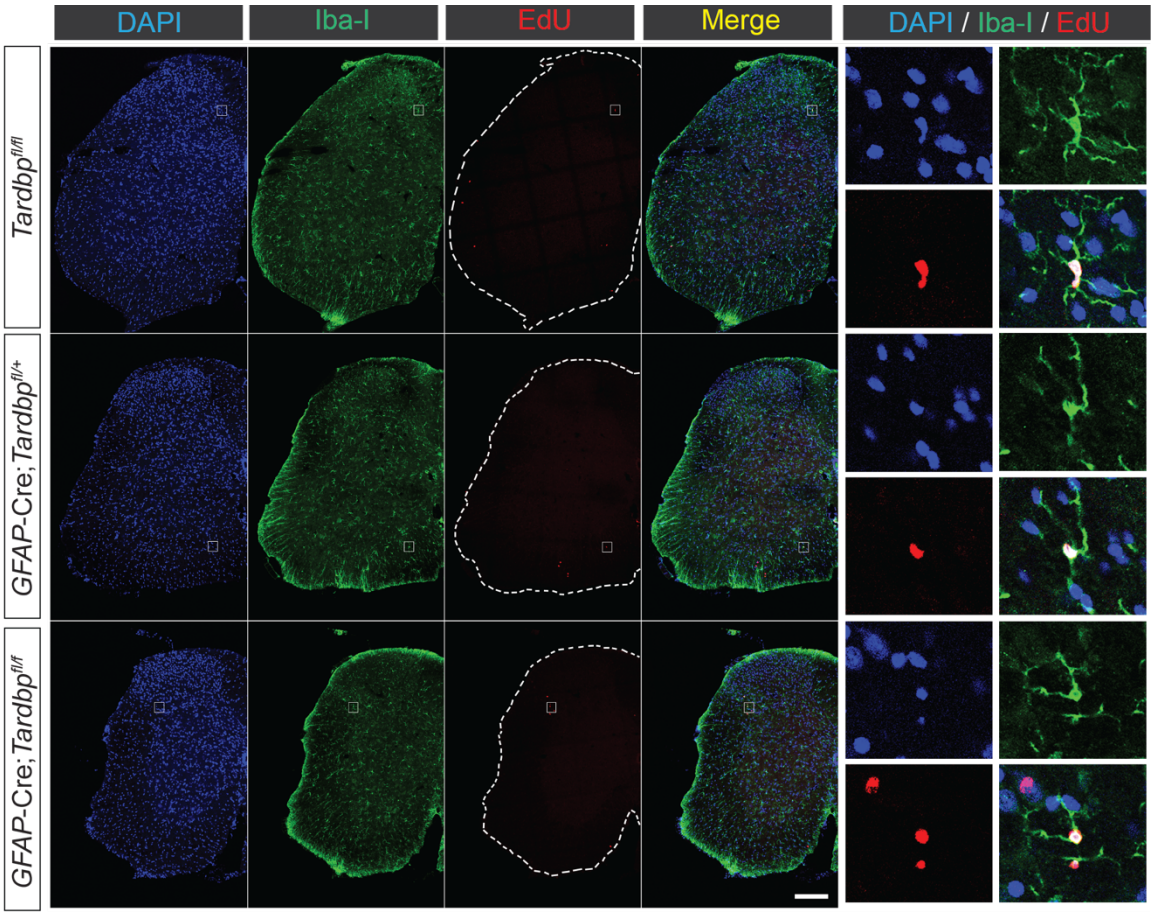

Fig. S5. No change in microglia proliferation in astroglial TDP-43 deletion mice

Fig. S5. No change in microglia proliferation in astroglial TDP-43 deletion mice. Confocal image of lumbar spinal cord of *Tardbp*$^{fl/fl}$ (ctr), *GFAP-Cre*;*Tardbp*$^{fl/+}$ (cHet), *GFAP-Cre*;*Tardbp*$^{fl/fl}$ (cKO) mice immuno-stained with microglia markers, Iba1 (green) with EdU (red). Blow-up images at the right to show the co-labeling of Iba1 and EdU microglia. Scale bar = 200 μm.

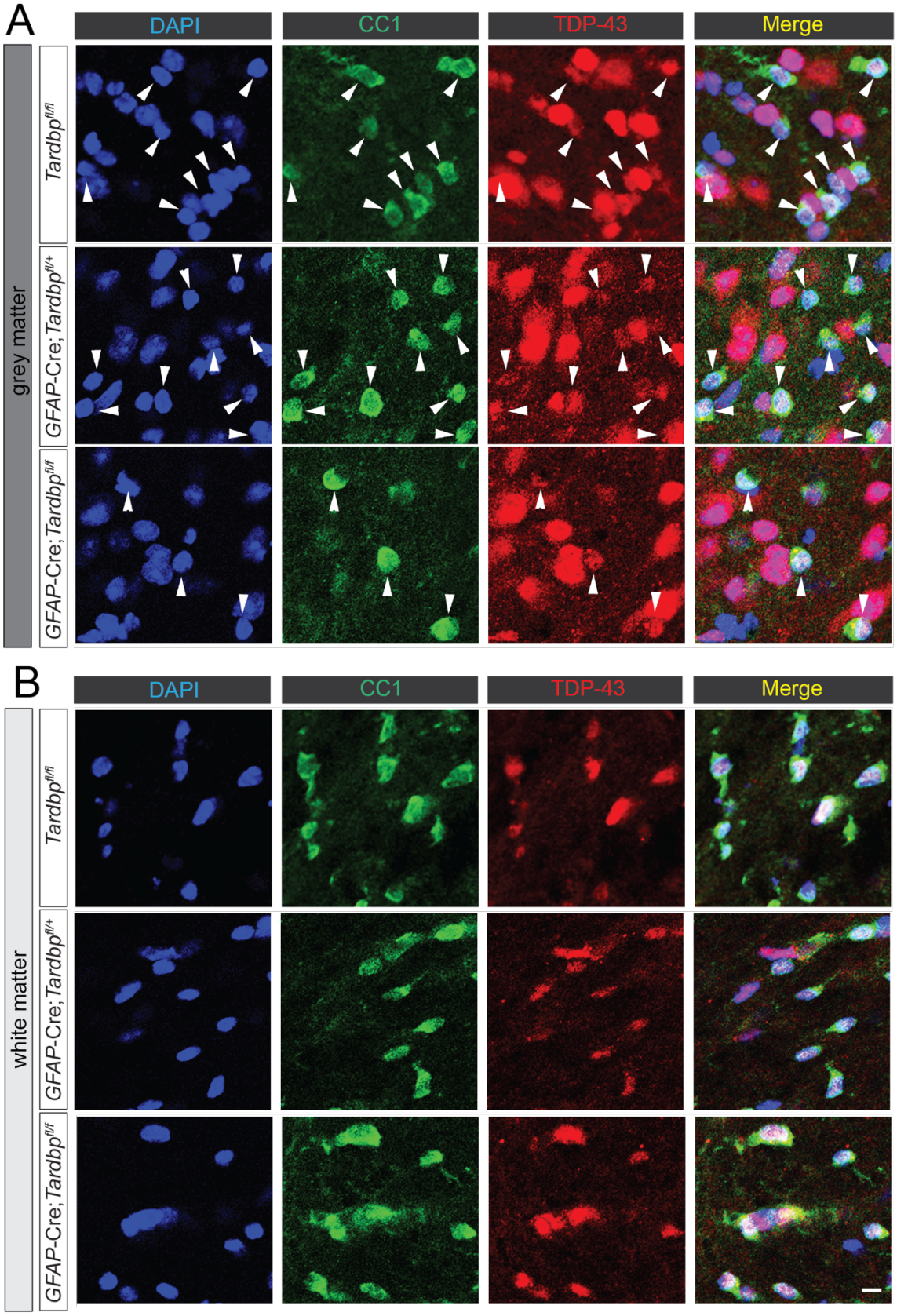

Fig. S6. Reduction of CC1-positive mature oligodendrocytes in astroglial TDP-43 deletion mice

Fig. S6. Reduction of CC1-positive oligodendrocytes in astroglial TDP-43 deletion mice. (A) Confocal image of the grey matter of lumbar spinal cord of *Tardbp*$^{fl/fl}$ (ctr), *GFAP-Cre*;*Tardbp*$^{fl/+}$ (cHet), *GFAP-Cre*;*Tardbp*$^{fl/fl}$ (cKO) mice immuno-stained with mature oligodendrocyte marker, APC-CC1 (green), with TDP-43 (red). (B) Confocal image of the white matter of lumbar spinal cord of *Tardbp*$^{fl/fl}$ (ctr), *GFAP-Cre*;*Tardbp*$^{fl/+}$ (cHet), *GFAP-Cre*;*Tardbp*$^{fl/fl}$ (cKO) mice immuno-stained with mature oligodendrocyte marker, APC-CC1 (green), with TDP-43 (red). Nuclei were stained with DAPI (blue). Scale bar = 20 μm.

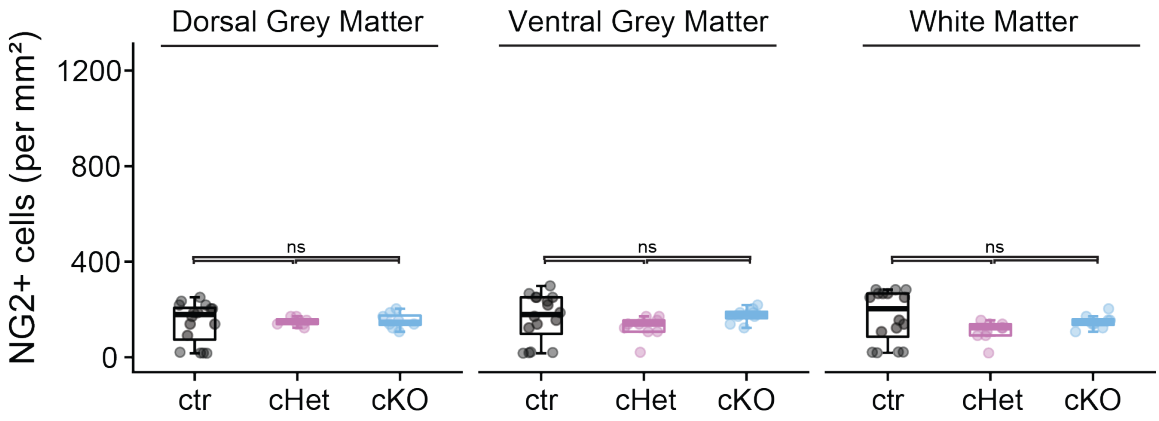

Fig. S7. No change in NG2-positive OPCs in astroglial TDP-43 deletion mice

Fig. S7. No change in number of NG2-positve OPCs in astroglial TDP-43 deletion mice. Quantification of EdU/NG2-double-positive OPCs in the lumbar spinal cords from *Tardbp*$^{fl/fl}$ (ctr), *GFAP-Cre*;*Tardbp*$^{fl/+}$ (cHet), *GFAP-Cre*;*Tardbp*$^{fl/fl}$ (cKO) mice. n=3 per genotype, at least 6 spinal cord slices per animal were analyzed. n.s.= not significant.

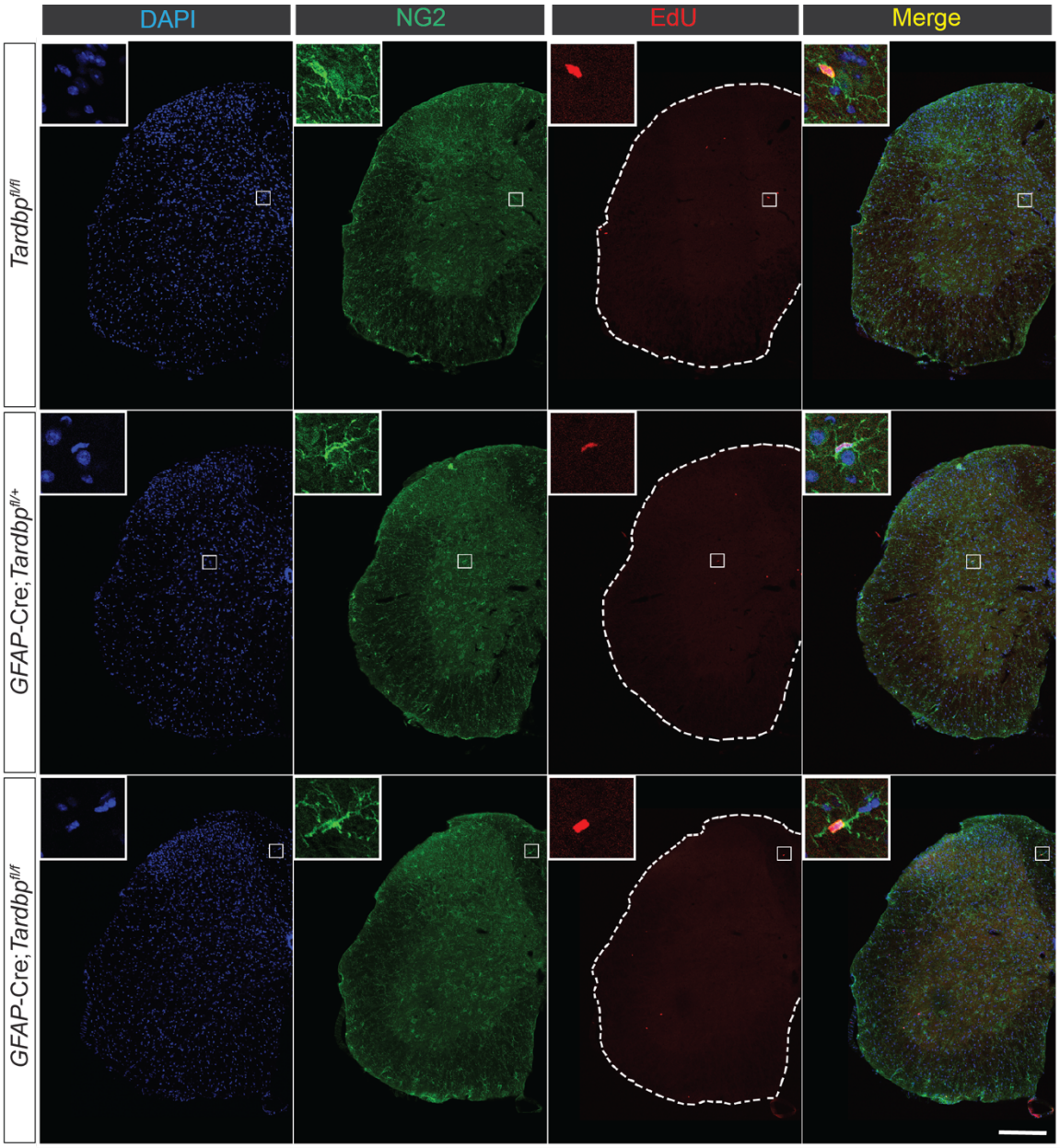

Fig. S8. No change in OPC proliferation in astroglial TDP-43 deletion mice

Fig. S8. No change of OPC proliferation in in astroglial TDP-43 deletion mice. Confocal image of lumbar spinal cord of *Tardbp*$^{fl/fl}$ (ctr), *GFAP-Cre*;*Tardbp*$^{fl/+}$ (cHet), *GFAP-Cre*;*Tardbp*$^{fl/fl}$ (cKO) mice immuno-stained with OPC markers, NG2 (green) with EdU (red). Enlarged images displayed on the right to show the co-labeling of NG2 and EdU OPC. Scale bar = 200 μm.

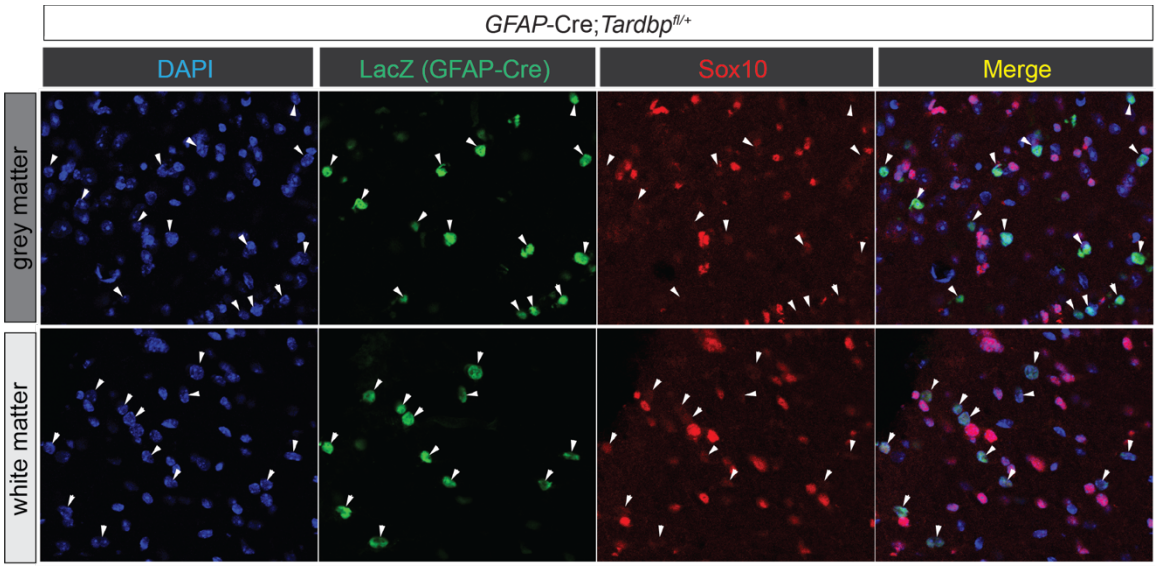

Fig. S9. Distinct cell population by LacZ and Sox10 staining

Fig. S9. Distinct cell population as labeld by LacZ and Sox10. Confocal image of lumbar spinal cord of *GFAP-Cre*;*Tardbp*$^{fl/+}$ (cHet) mice immuno-stained with LacZ (arrow, green) and Sox10 (red). *GFAP*-Cre transgene contains LacZ expression cassette, which can be identified by LacZ staining. LacZ and Sox10 stains distinct cell populations in both grey (upper panel) and white (lower panel) matter of the spinal cord.

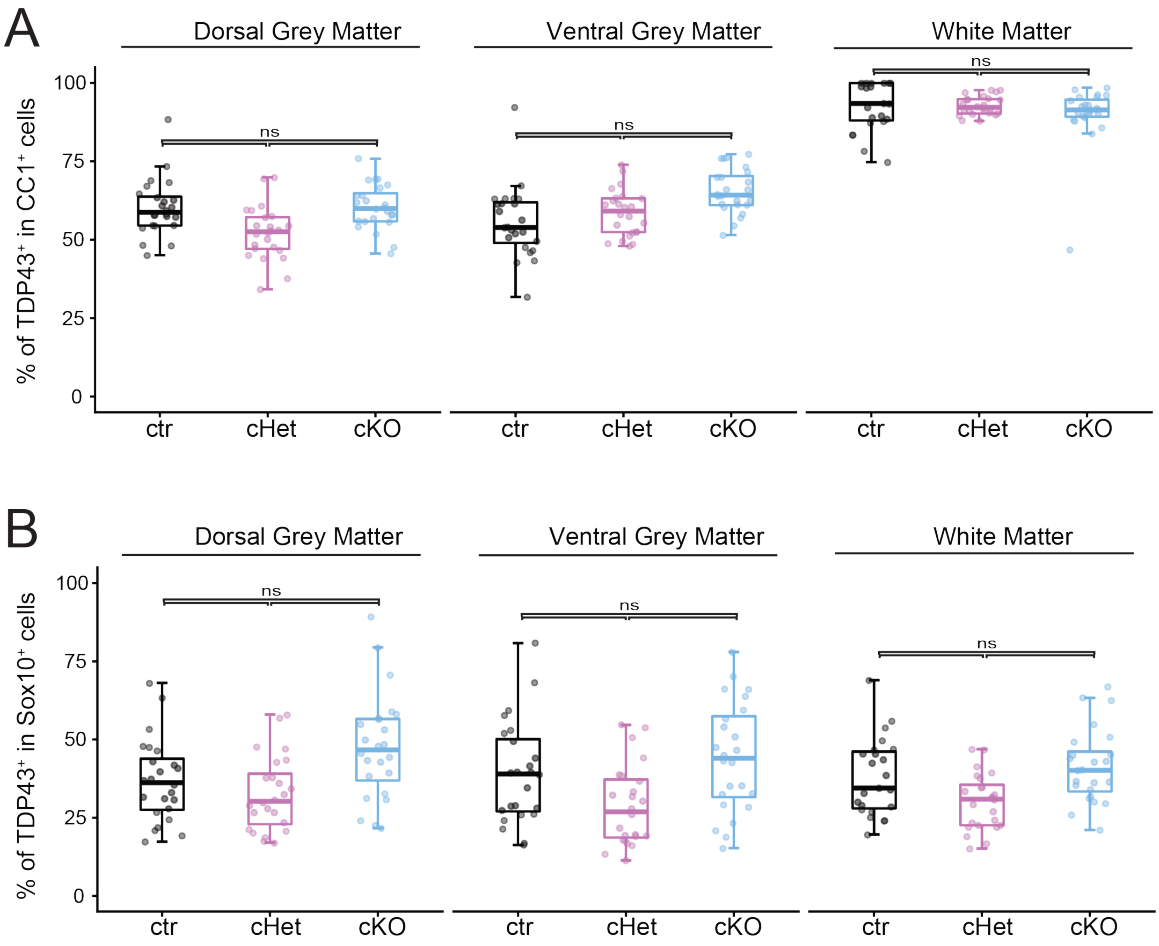

Fig. S10. No change in TDP-43 in CC1-positive oligodendrocytes and Sox10-postive oligodendrocyte lineage cells in astroglial TDP-43 deletion mice

Fig. S10. No change in the number of TDP-43 in CC1-positive oligodendrocytes and Sox10-positive oligodendrocyte lineage cells in astroglial TDP-43 deletion mice. (A) Quantification of percentage of TDP-43/CC1-double positive oligodendrocytes in the dorsal grey, ventral grey and white matter of lumbar spinal cords from *Tardbp*$^{fl/fl}$ (ctr), *GFAP-Cre*;*Tardbp*$^{fl/+}$ (cHet), *GFAP-Cre*;*Tardbp*$^{fl/fl}$ (cKO) mice. n=3 per genotype, at least 6 spinal cord slices per animal were analyzed. ns = not significant. (B) Quantification of percentage of TDP-43/Sox10-double positive oligodendrocyte lineage cells (OPCs to mature oligodendrocytes) in the dorsal grey, ventral grey and white matter of lumbar spinal cords from *Tardbp*$^{fl/fl}$ (ctr), *GFAP-Cre*;*Tardbp*$^{fl/+}$ (cHet), *GFAP-Cre*;*Tardbp*$^{fl/fl}$ (cKO) mice. n=3 per genotype, at least 6 spinal cord slices per animal were analyzed. ns = not significant.

Table S1: Primary antibodies used in this study

Antibody	Source	Catalog number	Concentration
Rabbit anti-GFAP	Proteintech	16825-1-AP	1:1000 (IF)
Goat anti-Sox9	R&D system	AF3075	1:1000 (IF)
Mouse anti-TDP-43	In-house	Ling et al., 2010 (1)	1:500 (IF)
Rabbit anti-TDP-43	Proteintech	10782-2-AP	1:500 (IF)
Rabbit anti-GFP	Proteintech	50430-2-AP	1:200 (IF)
Mouse anti-NeuN	Merck-Millipore	MAB377	1:1000 (IF)
Mouse anti-Olig2	Merck-Millipore	MABN50	1:500 (IF)
Goat anti-ChAT	Merck-Millipore	AB144P	1:200 (IF)
Rabbit anti-neurofilament-L	Cell Signaling Technology	2873	1:2000 (IF)
Rabbit anti-synaptophysin	Thermo Fisher Scientific	PA1-1043	1:300 (IF)
Rabbit anti-Iba1	Wako	019-19741	1:500 (IF)
Mouse anti-APC (CC1)	Merck-Millipore	OP80	1:200 (IF)
Rabbit anti-NG2	Merck-Millipore	AB5320	1:500 (IF)
Mouse anti-LacZ	Promega	Z3781	1:2000 (IF)
Goat anti-Sox10	R&D system	AF2864	1:500 (IF)

Table S2: Secondary antibodies used in this study

Antibody	Source	Catalog number	Concentration
Alexa Fluor™ 488 Donkey anti-mouse IgG (H+L)	Thermo Fisher Scientific	A21202	1:1,000 (IF)
Alexa Fluor™ 568 Donkey anti-mouse IgG (H+L)	Thermo Fisher Scientific	A10037	1:1,000 (IF)
Alexa Fluor™ 647 Donkey anti-mouse IgG (H+L)	Thermo Fisher Scientific	A31571	1:1,000 (IF)
Alexa Fluor™ 488 Donkey anti-rabbit IgG (H+L)	Thermo Fisher Scientific	A21206	1:1,000 (IF)
Alexa Fluor™ 568 Donkey anti-rabbit IgG (H+L)	Thermo Fisher Scientific	A10042	1:1,000 (IF)
Alexa Fluor™ 647 Donkey anti-rabbit IgG (H+L)	Thermo Fisher Scientific	A31573	1:1,000 (IF)
Alexa Fluor™ 488 Donkey anti-goat IgG (H+L)	Thermo Fisher Scientific	A11055	1:1,000 (IF)

Table S3: PCR primers used in this study

Target gene	**Forward primer sequence (5'-3')**	**Reverse primer sequence (5'-3')**
Mouse *C3*	CCAGCTCCCCATTAGCTCTG	GCACTTGCCTCTTTAGGAAGTC
Mouse *Serpina3n*	ATTTGTCCCAATGTCTGCGAA	TGGCTATCTTGGCTATAAAGGGG
Mouse *Ligp1*	CAGGACATCCGCCTTAACTGT	AGGAAGTAAGTACCCATTAGCCA
Mouse *C1qa*	CCACGGAGGCAGGGACACCA	CCGGGCGGCCAGGATTTC
Mouse *C1qb*	CACCAACGCGAACGAGAACTATGAG	CGCGGCCACGAACGAGATT
Mouse *Arhgdia*	CTCGGGGCAGTTACAACATCAAGTC	GTCGCCCTGCCCGTCTCC
Mouse *Gapdh*	AGGCCGGTGCTGAGTATGTCGTG	TCGGCAGAAGGGGCGGAGAT

Dataset S1: Statistic analysis for Figure 1-5

Dataset S2: Statistic analysis for Figure 6

SI References

1. S.-C. Ling, *et al.*, ALS-associated mutations in TDP-43 increase its stability and promote TDP-43 complexes with FUS/TLS. *Proc. Natl. Acad. Sci.* **107**, 13318–13323 (2010).